TICT compounds by design: comparison of two naphthalimide-π-dimethylaniline conjugates of different lengths and ground state geometries

Justina Jovaišaitė, Paulius Baronas, Gediminas Jonusauskas, Dalius Gudeika, Alytis Gruodis, Juozas Gražulevičius, Saulius Jursenas

TICT compounds by design: comparison of two naphthalimide-π-dimethylaniline conjugates of different lengths and ground state geometries

Justina Jovaišaitė, [a] Paulius Baronas, [a] Gediminas Jonusauskas, [b] Dalius Gudeika, [c] Alytis Gruodis,[d] Juozas V. Gražulevičius [c] and Saulius Juršėnas[a]

Two new twisted intramolecular charge transfer (TICT) donor-π-acceptor compounds were designed by combining a well-known electron acceptor naphthalimide unit with a classic electron donor dimethylaniline through two types of different rigid linkers. The combined steady-state and time-resolved spectroscopy of molecules in solvents of different polarities in comparison to solid-state solvation experiments of doped polymer matrixes of different polarities allowed distinguishing between solvation and conformation determined processes. The photophysical measurements revealed that non-polar solutions possess high fluorescence quantum yields of up to 70% which is a property of pre-twisted/planar molecules in the excited charge transfer (CT) states. The increase of polarity allows tuning the Stokes shift through all the visible wavelength range up to 8601 cm^{-1} which is accompanied by a three orders of magnitude drop of fluorescence quantum yields. This is a result of the emerged TICT states as dimethylaniline twists to a perpendicular position against the naphthalimide core. The TICT reaction of molecules enables an additional non-radiative excitation decay channel, which is not present if the twisting is forbidden in a rigid polymer matrix. Transient absorption spectroscopy was employed to visualize the excited state dynamics and to obtain the excited state reaction constants, revealing that TICT may occur from both the Franck-Condon region and the solvated pre-twisted/planar CT states. Both molecules undergo the same photophysical processes, however, a longer linker and thus a higher excited state dipole moment determines the faster excited state reactions.

Introduction

Organic π-conjugated molecules with electron donating (D) and electron accepting (A) characters represent so-called push-pull systems with an intramolecular charge transfer (CT) character which is essential to realize tuneable structural and functional properties for organic optoelectronic applications. The main strategy to design specific features of CT compounds comprises the appropriate selection of D and A moieties connected through π-conjugated linkers and the substitution position as well as the realization of planar/twisted and rigid/flexible molecular scaffolds. The conformational differences resulting in a perpendicular configuration of D and A fragments in the excited state may be further classified as a twisted intramolecular charge transfer (TICT) state, first proposed by Grabowski *et al.*[1] TICT states undergo full charge separation as twisting around the single bond leads to the deconjugation of electron donor and acceptor excited states, and are desirable for electrostatic force driven molecular motors, fluorescent molecular rotors, switches, probes, bioimaging, and lighting or even energy harvesting techniques.[2–4] Depending on the targeted application, both suppression and enhancement of TICT states could be required.[5]

In terms of molecular orbitals, the excited state geometry can be predicted considering several factors: (i) the HOMO–LUMO energy gaps between planar and twisted geometries; (ii) the difference in the hole-electron interactions; and (iii) the geometry relaxation of the excited state.[6] The first factor, mostly contributing to the formation of TICT, states that TICT is only possible if the twisted geometry has a smaller HOMO–LUMO

[a] *Institute of Photonics and Nanotechnology, Vilnius University, Saulėtekio Ave. 3, LT-10257 Vilnius, Lithuania. E-mail: justina.jovaisaite@ff.vu.lt*
[b] *Laboratoire Ondes et Matiére d'Aquitaine, Bordeaux University, UMR CNRS 5798, 351 cours de la Libération, 33405 Talence, France*
[c] *Department of Polymer Chemistry and Technology, Kaunas University of Technology, Radvilėnų rd. 19, LT-50254 Kaunas, Lithuania*
[d] *Institute of Chemical Physics, Vilnius University, Saulėtekio Ave. 3, LT-10257 Vilnius, Lithuania*

gap than that of a planar geometry, which can be favoured by strong HOMO–D and LUMO–A interactions.[6] Intuitively, TICT can be predicted by selecting an electron donor with a low ionization potential and an electron acceptor with a high electron affinity and an appropriate conjugation length between these two groups.[6] If TICT is favourable in a molecular system, it is more likely to occur in non-viscous, polar solvents due to the unrestricted molecular motions and better stabilization of polar charge transfer states.[7]

1,8-Naphthalimides (NIs), one of the well-known electron acceptors, are considered among the most important building blocks of efficient fluorescent materials.[8] Due to the relative simplicity of synthetic operations for targeted modification,[9,10] tuneable photophysical properties,[11] photostability,[12] thermostability[11,13] and biocompatibility,[14] NI materials have received tremendous attention from the scientific community and became a highly adaptable scaffold with a huge diversity of proposed real life applications.[15] These include studies demonstrating NI compounds as materials for optoelectronic devices (OLEDs, organic solar cells, logic gates),[16–21] as well as bio[22,23] and chemosensors[24–26] or even as fluorescent cell imaging agents.[27–30] Having in mind a redox potential of the 1,8-naphthalimide core (~ -1.8 V, *vs.* Ag/Ag$^+$),[31] many of the strategies for the mentioned applications cover the simple design of adding an electron donating substituent to the NI core at its 4th position to create donor–acceptor (D–A) type compounds with a CT character. One of the classic electron-donating substituents is *N*,*N*-dimethylaniline (DMA) with a redox potential of at least 0.65 V (*vs.* Ag/AgCl),[32] which may serve as a perfect charge donor with a high driving force for the intramolecular charge transfer upon combination with the NI core through selected linkers.

Thus, in this work, we present a comprehensive study of two new A-π-D fluorophores with electron acceptor NI and electron donor DMA fragments connected through two types of linkers at the 4th position of the NI core: single bond (**NA1**) or acetylene-like junction (**NA2**) (Fig. 1). Diverse pre-requisites (pre-twisted or planar ground state geometries as well as different conjugation lengths and different molecular dipolar moments in the excited state) were compared by steady-state and time-resolved spectroscopic methods; the transient absorption spectroscopy provided the main insights and allowed visualizing the dynamics of CT and TICT reactions, governed by environmental parameters (polarity and rigidity) and molecular properties. The supplementary studies of both compounds in rigid polymer matrices made it possible to clearly differentiate the spectral effects produced by dynamic solvation from those observed in the excited charge transfer states.

Results and discussion

DFT modelling, intramolecular charge transfer

Optimized ground state geometries and charge density distributions in the HOMO and LUMO states of compounds **NA1** and **NA2** in cyclohexane (CyHex) are depicted in Fig. 1. Both molecules reveal a CT nature of the electronic transition. The

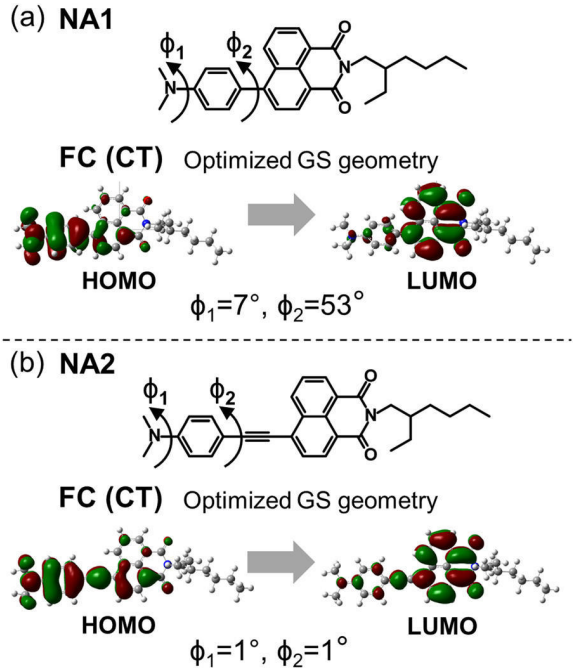

Fig. 1 Molecular structures and optimized ground state geometries with calculated electron density distributions for HOMO and LUMO molecular orbitals of compounds **NA1** (a) and **NA2** (b) in cyclohexane.

HOMO state comprises charge redistribution between NI and DMA moieties, while the charge density in the LUMO state is localized mainly on the NI core. The studied compounds show different twist angles between NI and DMA moieties. Compound **NA1** with phenyl ring as a π-linker has a pre-twisted geometry in a ground state: the twist angle between dimethylamine and benzene (ϕ_1) is 7°, while between NI and DMA (ϕ_2) is 53°. Compound **NA2** with the phenyl-acetylene junction possesses a planar ground state geometry.

CT and TICT states probed by steady-state and time-resolved fluorescence spectroscopy

Normalized absorption and fluorescence spectra of **NA1** and **NA2** in a range of aprotic solvents are depicted in Fig. 2. Photophysical data obtained by steady-state and time-resolved fluorescence experiments are summarized in Table 1.

As already predicted from molecular structures (A-π-D), both molecules exhibit photophysical properties characteristic to CT states. The absorption spectra are comprised of higher energy bands, typical of dimethylaniline (285–313 nm),[33] 1,8-naphthalimide (350 nm)[8,34] fragment absorption and the CT state absorption at 407–448 nm in various solutions, also observed for similar D–A naphthalimide derivatives.[11,34,35] The structureless absorption band of **NA1** and a clear vibronic structure of **NA2** in CyHex confirm the pre-twisted and planar ground state geometries, respectively. Upon increasing the polarity of the solvent, a slight red-shift and a gradual

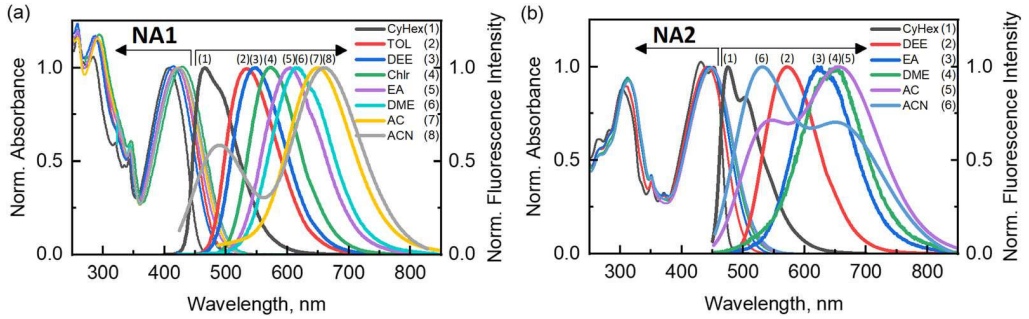

Fig. 2 Normalized absorption and fluorescence spectra of compounds **NA1** (a) and **NA2** (b) in different solvents: cyclohexane (CyHex), toluene (TOL), diethyl ether (DEE), chloroform (Chlr), ethyl acetate (EA), dimethoxyethane (DME), acetone (AC) and acetonitrile (ACN). Samples were excited at 420 nm. The legend denotes solvent name abbreviations. The plotted emission spectra of **NA1** in acetonitrile and **NA2** in acetone and acetonitrile are Gaussian fits of experimental data,

Table 1 Steady-state absorption, fluorescence and time-resolved fluorescence data of compounds **NA1** and **NA2** in solvents of different polarizabilities and polymer matrixes of different polarities, obtained by exciting samples at 420 nm

	Solvent	ε	Δf [a]	λ_{ABS}, [b] nm	λ_{FL}, [c] nm	$\Delta\nu$, [d] cm^{-1}	Φ_{FL}, [e] %	τ, [f] ns	τ_r, [g] ns	τ_n, [h] ns
NA1	Cyclohexane (CyHex)	2.02	0.100	407	465	3255	73	3.45	4.70	12.96
	Diethyl ether (DEE)	4.33	0.256	414	547	6083	39	6.25	15.99	10.26
	Ethyl acetate (EA)	6.02	0.292	420	605	7397	6.5	2.96	45.24	3.17
	Dimethoxyethane (DME)	7.2	0.309	423	616	7539	3.0	0.84	28.14	0.86
	Acetone (AC)	20.7	0.374	423	651	8456	0.45	0.17	37.18	0.17
	Acetonitrile (ACN)	37.5	0.393	424	490, 661	3430, 8601	0.1 (0.03/0.07) [j]	0.01/0.07 [k]	21.18/98.22	0.01/0.07
	1% wt in polystyrene (PS)	2.45 [i]	—	428	519	4190	76	6	7.83	24.79
	1% wt in PMMA (PMMA)	3.41 [i]	—	428	544	5274	56	8	14.29	18.18
	1% wt in PMMA, 20% wt of CA (PMMA/CA)	8.31 [i]	—	431	578	6170	41	9.5	23.17	16.1
NA2	Cyclohexane (CyHex)	2.02	0.100	452	475	1203	71	2.41	3.38	8.42
	Diethyl ether (DEE)	4.33	0.256	443	572	5302	26	4.05	15.63	5.47
	Ethyl acetate (EA)	6.02	0.292	445	631	6711	0.71	0.50	70.32	0.50
	Dimethoxyethane (DME)	7.2	0.309	449	652	6958	0.27	0.25	92.94	0.25
	Acetone (AC)	20.7	0.374	448	538, 662	3991, 7448	0.06 (0.02/0.04) [j]	<0.002/0.04 [l]		
	Acetonitrile (ACN)	37.5	0.393	448	529, 667	3688, 7579	0.03 (0.02/0.01) [j]	<0.002/0.04 [l]		
	1% wt in polystyrene (PS)	2.45 [i]	—	459	546	3578	68	5	6.94	14.75
	1% wt in PMMA (PMMA)	3.41 [i]	—	452	578	4961	44	6	13.64	10.71
	1% wt in PMMA, 20% wt of CA (PMMA/CA)	8.31 [i]	—	456	610	5818	33	5.5	16.67	8.21

[a] Solvent-dependent parameter according to Weller's equation, $\Delta f = \frac{\varepsilon - 1}{2\varepsilon + 1} - \frac{n^2 - 1}{4n^2 + 2}$. Here, ε is a static dielectric constant and n is a refractive index of the solvent. [b] Wavelength of the lowest energy absorption maxima. [c] Wavelength of the fluorescence spectra maxima. Excitation wavelength was set to 420 nm. [d] Stokes shift. [e] Fluorescence quantum yields. [f] Fluorescence lifetimes. [g] $\tau_{rad} = \frac{\tau}{QY}$. [h] $\tau_{nonrad} = \frac{\tau}{1 - QY}$. [i] The dielectric constant values were taken from ref. 37. [j] The fluorescence quantum yield values in parenthesis correspond to the blue and red side fluorescence bands. [k] Two fluorescence lifetimes were recorded at maxima of dual fluorescence peaks (517 nm/663 nm). [l] The fluorescence decay transients of **NA2** in AC and ACN could be fitted bi-exponentially. Here only longer lifetime values are given as the fast components are below the equipment's temporal resolution.

broadening of absorption spectra are observed for both molecules. The absorption spectral changes mainly suggest that absorption solvatochromism of the pre-twisted **NA1** is mostly related to slightly different ground state geometries. In terms of planar **NA2**, its dipole moments in ground state (as well as in the excited Franck–Condon state) are roughly the same and thus, only a minor absorption spectral red-shift of a few nanometres is observed[36]

The CT character of NI compounds ensures the significant dependence of fluorescence properties on solvent polarizability. In CyHex, both compounds already exhibit a large Stokes shift of 3255 cm^{-1} (**NA1**) and 1203 cm^{-1} (**NA2**), respectively, pointing towards the fluorescence from CT states even in a non-polar environment. The smaller Stokes shift and more pronounced vibronic shape of fluorescence spectra of **NA2** show the planar excited state geometry in a non-polar solvent. In the case of **NA1**, the fluorescence spectrum in CyHex also possesses a vibronic shape. This may be related to the partial planarization of the molecule's geometry after photoexcitation in a non-polar environment. The planarization of **NA1** is also supported by the excited state optimization calculations, which show the decrease of the dihedral angle between NI and DMA moieties to *ca.* 30°

Even the small increase of the solvent's dielectric constant up to ε = 4.33 (diethyl ether, DEE) determines the pronounced

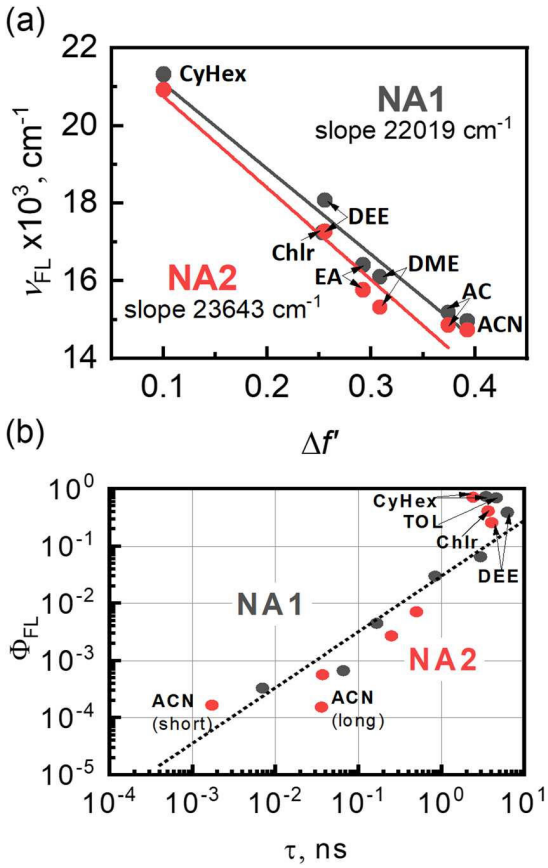

Fig. 3 Weller's polarity plots of compounds **NA1** (black dots) and **NA2** (red dots) (a). The black and red lines represent the best linear fits. Only red bands of fluorescence spectra are included for **NA1** in ACN and **NA2** in AC and ACN. Fluorescence quantum yields (Φ_{FL}) *versus* fluorescence lifetimes (τ) for **NA1** (black dots) and **NA2** (red dots) (b). The dotted line represents a slope equal to 1 in a log–log scale.

Stokes shift of 6083-5302 cm^{-1} which becomes as large as 8601–7579 cm^{-1} in most polar tested environment with ε = 37.5 (acetonitrile, ACN) for **NA1–NA2**, respectively. The dynamics of absorption and fluorescence spectra of **NA1** and **NA2** already suggests the increase of molecules' dipole moment upon excitation.[35] The excited state dipole moments (μ_e) of compounds were evaluated by a modified Lippert-Mataga approach, called Weller's equation[38]

, that accounts for fluorescence solvatochromic effects only. The estimated μ_e is 20 D for **NA1** and 22.5 D for **NA2**. The obtained excited state values are twice as high as the calculated ground state dipole moments and indicate a strong charge transfer character of compounds. Thus, not only different geometries but also different μ_e are the molecular prerequisites for the excited state dynamics.

The pronounced fluorescence spectral shift is accompanied by significant changes in fluorescence quantum yields (Φ_{FL}) and lifetimes (τ) (Table 1). The high value of Φ_{FL} in CyHex of *ca.* 70% drops to 39% (**NA1**) and 26% (**NA2**) in DEE. At the same time, the slight increase in solvents polarity prolongs fluorescence lifetimes by a factor of two: from 3.4 ns (CyHex) to 6.3 ns (DEE) for **NA1** and from 2.4 ns to 4.1 ns for **NA2**. A further increase of solvent dielectric constant leads to a further Φ_{FL} drop (down to 6.5% for **NA1** and to 0.7% for **NA2** in EA) and, interestingly, a decrease of fluorescence lifetimes (τ = 3 ns and τ = 0.5 ns for **NA1** and **NA2** in EA). Thus, from a certain dielectric constant of the solvent (ε = 6.02), the opposite trend of fluorescence lifetime behaviour is observed, where non-radiative excitation decay starts to dominate. The most polar environment (AC and ACN) determines almost forbidden (QY < 1%) dual fluorescence with extremely short τ values of tens of picoseconds (τ = 70 ps for **NA1** and τ = 40 ps for **NA2**, ACN). One has to note that the dual fluorescence in AC and ACN is of very low intensity, and thus, the impact of the emission from two different states (*e.g.*, determined by different geometries) as well as the impact of the impurities may have been observed.

The fluorescence quantum yields *versus* fluorescence lifetimes, shown in Fig. 3b, nicely illustrate the discussed trends. A negative slope of $\Phi_{FL}(\tau)$ is observed in CyHex, DEE, toluene (TOL), and chloroform (Chlr), while for the rest of the tested more polar solvents (ε > 6) a positive slope close to 1 is determined. These two distinct tendencies of Φ_{FL} *versus* τ as well as a significant Stokes shift accompanied by the drop in both fluorescence quantum yields as well as their lifetimes cannot be explained by the excited charge transfer states itself. We suggest that the observed photophysical properties of NI compounds arise from the competition between pre-twisted or planar CT states and TICT, that become dominant in solvents with ε > 6. The fluorescence in most polar solvents, however, can be observed due to the conformational disorder of twist angles near 90° at room temperature. In order to distinguish between solvation and twisting determined processes/properties in solvents, we further employed solid-state solvation experiments in rigid polymer matrixes with different dielectric constants, where molecular motions would be highly restricted.

Three different rigid systems were employed to obtain the set of polymer samples of different dielectric constants that were doped with **NA1** and **NA2** compounds: 1 wt% polystyrene (PS) (ε = 2.45), 1 wt% poly(methyl methacrylate) (PMMA) (ε = 3.41) and 1 wt% PMMA with 20 wt% of camphoric anhydrite (PMMA/CA) (ε = 8.31).[37] The CA was selected as a co-dopant for polymeric samples due to its small size and high ground state dipole moment in order to realize the solid-state solvation effect.[37,39] Upon the increase of polymer matrix polarity, the gradual red-shift of fluorescence spectra was observed . Contrary to the obtained results in solutions, only a slight decrease of Φ_{FL} (from 76% in PS to 41% in PMMA/CA for **NA1** and from 68% to 33% for **NA2**) along with slightly prolonged fluorescence lifetimes (6 ns to 9.5 ns for **NA1** and 5 ns to 6 ns for **NA2**) were observed in a rigid environment. Thus, the obtained results in polymeric films confirm that the efficient non-radiative decay channel is enabled only in polar solvents and is mainly related to geometry changes. One has to note that the decrease of fluorescence lifetimes in solvents is not a TICT property itself but should be considered as an outcome of an efficient non-radiative decay channel that is enabled by the twisted geometry, whether

through an efficient coupling with a dense manifold of polar solvent vibrational states[40,41] or, alternatively, through the intersection of the excited singlet state potential surface with triplet states.

So far, it is evident that the excited state relaxation dynamics of studied naphthalimide compounds highly depends on the solvent-fluorophore interaction as well as the viscosity of the environment. The more efficient non-radiative excitation decay channel of **NA2** and a more pronounced decrease of fluorescence quantum yields upon an increase of solvents' polarity correlate well with a higher excited state dipole moment μ_e. However, no influence of the pre-twisted geometry of **NA1** was observed. In order to get deeper insights into excited CT/TICT state dynamics, we further employed transient absorption spectroscopy experiments.

Transient absorption spectroscopy: the solvation dynamics and TICT reaction rates

The obtained picosecond time scale transient absorption (TA) maps and spectra in solvents of different polarity (CyHex, TOL, EA and ACN) (Fig. 4) illustrate the competition between pre-twisted/planar and twisted geometries upon excitation at the CT absorption band, confirming the results obtained by steady-state and time-resolved fluorescence spectroscopy.

The initially recorded spectra of **NA1** (**NA2**) in CyHex are already of charge transfer nature and comprise the excited state

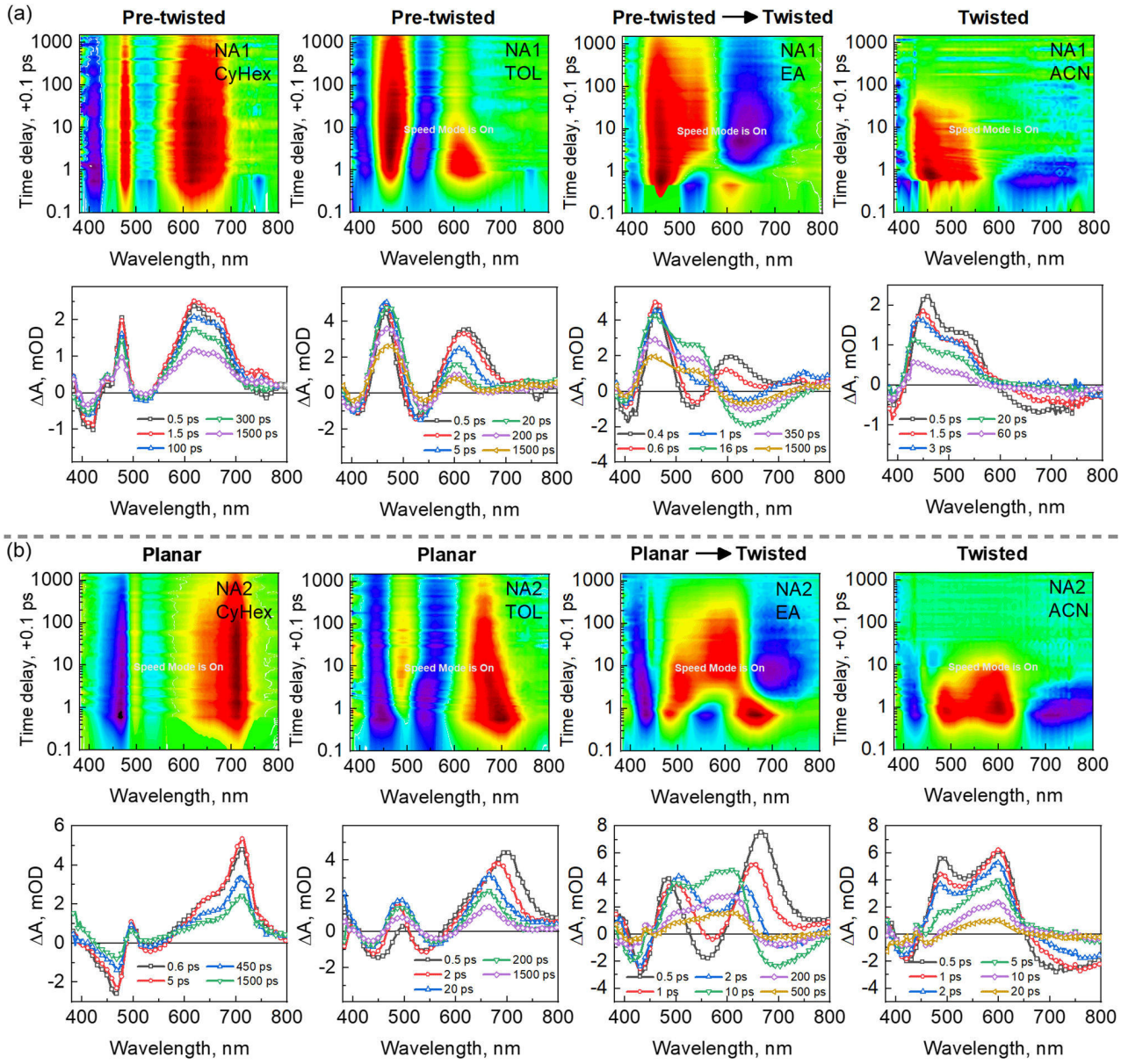

Fig. 4 Time-resolved transient absorption maps of **NA1** (a) and **NA2** (b) in cyclohexane (CyHex), toluene (TOL), ethyl acetate (EA) and acetonitrile (ACN), and its corresponding spectra at a given time delay. Samples were excited at 420 nm.

absorption (ESA) observed at 460 nm (500 nm), similar to 1,8-naphthalimide S_1 state absorption spectra,[42] also, at 620 nm (650) and at 660 nm (710 nm). ESA of both compounds significantly overlaps with signals of ground state bleaching (GSB) at *ca.* 400 nm (450 nm) and signals of negative nature, related to stimulated emission (SE) that appear at *ca.* 500 nm (520 nm). No pronounced dynamic solvation was observed in a non-polar environment, as expected. In slightly more polar TOL, the dynamic solvation with a time constant of 2.6 ps[43] takes place, which is nicely illustrated by the spectral shifts for both compounds: signals of SE shift to the red side of spectra, while ESA observed at around 600 nm undergoes the blue-shift. The TA spectral shape observed in a non-polar environment is attributed to partially twisted or planar CT states, as also discussed in the previous section.

The most interesting, though, complex, excited state relaxation dynamics is observed in more polar EA. The initial TA spectra are similar to those observed in less polar solvents. Clearly, spectral shifts occur in time and are characteristic of dynamic solvation with an EA re-orientation time constant of 0.86 ps.[43] Besides, the new spectral component starts to form even earlier than the dynamic solvation is completed and only at the time delay of 16 ps for **NA1** and 10 ps for **NA2** it is completely formed and has a lifetime similar to those observed in time-resolved fluorescence measurements.

One could argue whether the observed changes in TA maps in EA are attributed to geometry changes (planar *vs.* twisted, where full charge separation takes place) or are mainly related to solvation (*i.e.*, the negative band shifts to the red and so the positive band at 500 nm could be observed, which was not possible due to spectral band overlap before solvation took place). Thus, the TA experiments were repeated for samples in PMMA and PMMA/CA. At different time delays of 1 ps and 100 ps, the slight spectral shifts are only observed (Fig. 5a and c). The comparison of results in EA and PMMA/CA (Fig. 5b and d) clearly demonstrates that transient absorption spectra of

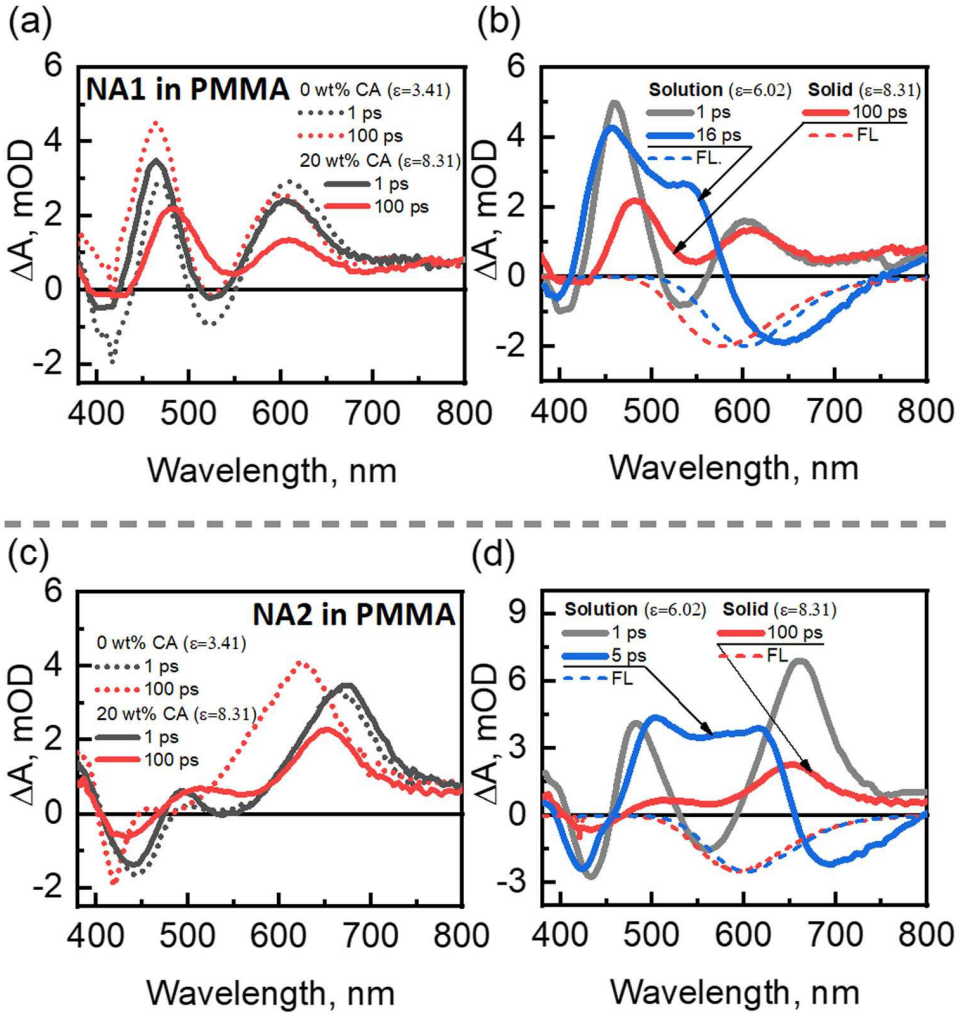

Fig. 5 Transient absorption spectra in 1 wt% PMMA (0 wt% CA) (dotted lines) and 1 wt% PMMA with 20 wt% CA (20 wt% CA) (solid lines) at 1 ps (black) and 100 ps (red) time delays of **NA1** (a) and **NA2** (c). The transient absorption spectra in ethyl acetate (solution) at 1 ps (grey lines) and at 16 ps or 5 ps (blue solid lines) in comparison with TA spectra in 1 wt% PMMA with 20 wt% CA (solid) at 100 ps time delay (red solid line) of **NA1** (b) and **NA2** (d). The dashed red and blue lines in (b) and (d) represent inverted normalized fluorescence spectra respective to solvents or films. Samples were excited at 420 nm.

NA1 and **NA2** in polar polymer resemble those obtained for a solution at early time delay (1 ps) rather than the one after dynamic solvation along with TICT reaction is completed. Consequently, the "new" spectral shapes at 16 ps for **NA1** and 10 ps for **NA2** are attributed to the excited TICT states. However, even if TICT should determine the complete charge separation, the observed spectra in EA (and ACN) are not formally bi-radical TA spectra as stimulated emission exists and has the same lifetime as ESA components. As mentioned previously, the emission from TICT states may be allowed due to the disorder of naphthalimide-dimethylaniline twist angles near 90°. The dynamic solvation in most polar ACN solvents happens in 0.26 ps,[43] thus, due to the temporal resolution of the experiment, the initial shape of TA spectra for both **NA1** and **NA2** is already an outcome of dynamic solvation and TICT reaction (Fig. 4).

To evaluate the pathways that lead to the formation of twisted charge transfer states, global analysis (GA) together with a target analysis of transient absorption data was employed.[44,45] GA was performed for **NA1** and **NA2** in EA by applying the sequential model including 3 (**NA1**) or 4 (**NA2**) compartments . The GA was applied up to 16 or 10 ps time delay in order to simplify the model and to account only for the early time-scale excited state dynamics. The obtained evolution associated spectra (EAS) highly resemble the particular TA spectra obtained in other environments (non-polar or polar solvents, or solid state). The EAS of the first compartment are similar to non-solvated TA spectra obtained in CyHex or TOL, while the EAS of 3rd (or 4th compartments in case of **NA2**) are analogous to TA spectra in most polar ACN, corresponding to the TICT state (Fig. 4). The intermediate states of the 2nd compartment for both compounds remind the solvated state as it was seen in polar polymer samples (Fig. 5). However, in terms of EAS, they are clearly affected by an additional process.

As it was already shown in a work of Park *et al.* that the TICT state can be reached through several pathways for a classic DMABN compound (*e.g.*, from locally excited or from partially twisted states),[46] the applied sequential model was updated by including a parallel process, which presumably could correspond to a different channel for the TICT state to be formed. Again, 3 or 4 compartments were included for a reasonable fit for **NA1** and **NA2** molecules, respectively (Fig. 6). The obtained decay associated spectra were similar to EAS, as recently discussed. Thus, we associate the included compartments to the excited singlet charge transfer state in a Frack–Condon region (S_{FC}) of a ground state geometry, the intermediate state that corresponds to the solvated CT state (S_{CT}) (*i.e.*, the excited state that forms after the dynamic solvation) and TICT states (S_{TICT}). In the case of **NA2**, the 4th compartment represents a possible formation of the second oriented solvent shell around the elongated dipole in the **NA2** TICT state. It is quite possible that the molecular structure of **NA2** may accept a few additional solvent molecules in the space between D and A since the distance separating these is almost 2.4 Å longer than in **NA1**. An evolution of the transient spectra

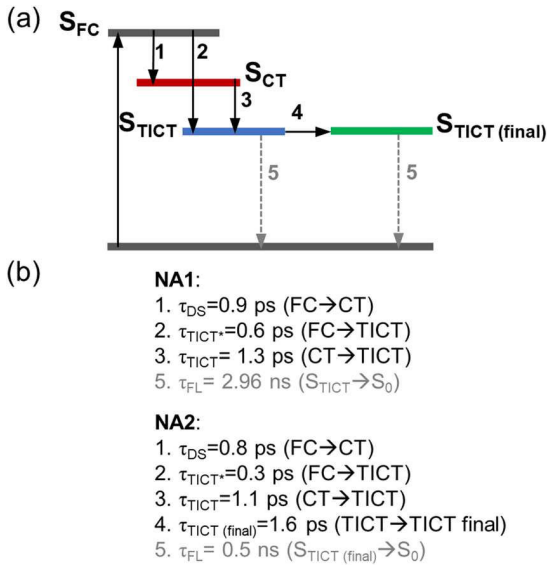

Fig. 6 The simplified model employed to perform the Global Analysis for the TA measurements of **NA1** and **NA2** in ethyl acetate (a). Model includes the excited Franck–Condon state (S_{FC}), the excited solvated charge transfer state (S_{CT}), the excited twisted intramolecular charge transfer state (S_{TICT}) and the final TICT state for **NA2** ($S_{TICT\ (final)}$). The punctured arrows are included for clarity to demonstrate the completion of the excited state reactions, *i.e.*, the relaxation of excited twisted molecules to the ground state. The obtained reaction rates for **NA1** and **NA2** are given in (b). The values of fluorescence lifetimes (τ_{FL}) were taken from time-resolved fluorescence experiments.

of **NA1** in EA contains an isosbestic point at 570 nm contrary to **NA2** where the isosbestic point disappears after 2 ps of spectral evolution (Fig. 4). The global and target analysis shows that the solvated excited state (S_{CT}) is reached within 0.8–0.9 ps that matches the EA re-orientation time constant. The TICT state (S_{TICT}) may be formed directly from the Franck–Condon region with τ_{TICT*} = 0.6 ps (or 0.3 ps for **NA2**) or from the solvated CT state with τ_{TICT} = 1.3 ps (1.1 ps), meaning that molecules have two different pathways to reach perpendicular geometry, and TICT, in fact, may occur earlier than dynamic solvation is completed.

Thus, the TA results in non-polar CyHex and TOL represent excitation relaxation in CT states of partially twisted or planar geometries, while the results in middle polar EA show the competition between CT and TICT, and finally, the TA spectra in ACN correspond to the dominant TICT. These findings nicely match the earlier discussed results obtained by steady-state and time-resolved fluorescence experiments, suggesting the twisting starts to occur in solvents of middle polarity. As is seen from Fig. 4, the increased reaction rates of TICT in a more polar environment cause more pronounced fluorescence quenching. The dynamic solvation determines whether twisting occurs; however, its reaction rate does not outcompete the reaction rate of TICT. We see that conjugation length and, yet, the higher polarity of molecules may cause the TICT reaction to occur slightly faster. Again, no signs of the influence of pre-twisted geometry are observed.

Conclusions

To sum up, two naphthalimide-dimethylaniline A-π-D molecules were thoroughly studied in terms of their photophysical behaviours in solvents and polymer matrixes of different polarities. Both molecules demonstrate a charge transfer character whether in partially planar/planar or twisted excited state geometries, which significantly depends on the parameters of the environment. The molecules are pre-twisted or planar in non-polar solvents and thus, high fluorescence quantum yields of up to 70% were achieved. However, the increase of solvent polarity determines the competition between CT and TICT states. Once TICT state is dominant in solvents with $\varepsilon > 6$, the efficient non-radiative decay channel is enabled which determines up to three orders of magnitude drop in fluorescence quantum yields and the decreased fluorescence lifetimes. In contrast, in the polymer matrix of similar polarity, the fluorescence quantum yields remain comparatively high (*ca.* 30% – 40%) along with slightly increased fluorescence lifetimes due to more stabilized CT states. The transient absorption spectroscopy confirmed the results obtained by steady-state and time-resolved fluorescence measurements and revealed that different channels exist to reach TICT states: whether from the CT states in the Franck–Condon region or from the solvated CT states. In case TICT is formed directly from the FC region, its reaction rate outcompetes the dynamic solvation. The pre-twisted geometry of the compound has no influence in terms of excited state reaction rates. On the other hand, the higher excited state dipole moment determines the faster excited state processes.

Conflicts of interest

There are no conflicts to declare.

Acknowledgements

We thank dr. Rokas Skaisgiris for the contribution at the early stages of the project. We also thank dr. Karolis Šarka for the insights on theoretical modelling. Computations were performed on resources at the High Performance Computing Centre "HPC Saulėtekis" in Vilnius University, Faculty of Physics.

References

1 Z. R. Grabowski, K. Rotkiewicz and A. Siemiarczuk, *J. Lumin.*, 1979, **18–19**, 420–424.
2 E. Y. Chernikova, D. V. Berdnikova, Y. V. Fedorov, O. A. Fedorova, F. Maurel and G. Jonusauskas, *Phys. Chem. Chem. Phys.*, 2017, **19**, 25834–25839.
3 S. Sasaki, G. P. C. Drummen and G. Konishi, *J. Mater. Chem. C*, 2016, **4**, 2731–2743.
4 S. C. Lee, J. Heo, H. C. Woo, J. A. Lee, Y. H. Seo, C. L. Lee, S. Kim and O. P. Kwon, *Chem. – Eur. J.*, 2018, **24**, 13706–13718.
5 C. Wang, W. Chi, Q. Qiao, D. Tan, Z. Xu and X. Liu, *Chem. Soc. Rev.*, 2021, **50**, 12656–12678.
6 C. Zhong, *Phys. Chem. Chem. Phys.*, 2015, **17**, 9248–9257.
7 A. Nandi, R. Ghosh and D. K. Palit, *J. Photochem. Photobiol., A*, 2016, **321**, 171–179.
8 D. Jacquemin, E. A. Perpète, G. Scalmani, I. Ciofini, C. Peltier and C. Adamo, *Chem. Phys.*, 2010, **372**, 61–66.
9 N. V. Marinova, N. I. Georgiev and V. B. Bojinov, *J. Photochem. Photobiol., A*, 2013, **254**, 54–61.
10 M. Oelgemöller and W. H. Kramer, *J. Photochem. Photobiol., C*, 2010, **11**, 210–244.
11 D. Gudeika, J. V. Grazulevicius, G. Sini, A. Bucinskas, V. Jankauskas, A. Miasojedovas and S. Jursenas, *Dyes Pigm.*, 2014, **106**, 58–70.
12 V. B. Bojinov, N. I. Georgiev and N. V. Marinova, *Sens. Actuators, B*, 2010, **148**, 6–16.
13 D. Gudeika, A. Michaleviciute, J. V. Grazulevicius, R. Lygaitis, S. Grigalevicius, V. Jankauskas, A. Miasojedovas, S. Jursenas and G. Sini, *J. Phys. Chem. C*, 2012, **116**, 14811–14819.
14 S. Y. Xu, X. Sun, H. Ge, R. L. Arrowsmith, J. S. Fossey, S. I. Pascu, Y. B. Jiang and T. D. James, *Org. Biomol. Chem.*, 2015, **13**, 4143–4148.
15 P. Gopikrishna, N. Meher and P. K. Iyer, *ACS Appl. Mater. Interfaces*, 2018, **10**, 12081–12111.
16 W. Zeng, H. Y. Lai, W. K. Lee, M. Jiao, Y. J. Shiu, C. Zhong, S. Gong, T. Zhou, G. Xie, M. Sarma, K. T. Wong, C. C. Wu and C. Yang, *Adv. Mater.*, 2018, **30**, 1704961.
17 W. Chai and R. Jin, *J. Mol. Struct.*, 2016, **1103**, 177–182.
18 D. Gudeika, *Synth. Met.*, 2020, **262**, 116328.
19 W. Zhang, Y. Xu, M. Hanif, S. Zhang, J. Zhou, D. Hu, Z. Xie and Y. Ma, *J. Phys. Chem. C*, 2017, **121**, 23218–23223.
20 B. Wang, Y. Zheng, T. Wang, D. Ma and Q. Wang, *Org. Electron.*, 2021, **88**, 106012.
21 C. J. Christopherson, D. M. Mayder, J. Poisson, N. R. Paisley, C. M. Tonge and Z. M. Hudson, *ACS Appl. Mater. Interfaces*, 2020, **12**, 20000–20011.
22 L. Zhou, L. Xie, C. Liu and Y. Xiao, *Chin. Chem. Lett.*, 2019, **30**, 1799–1808.
23 C. Geraghty, C. Wynne and R. B. P. Elmes, *Coord. Chem. Rev.*, 2021, **437**, 213713.
24 R. M. Duke, E. B. Veale, F. M. Pfeffer, P. E. Kruger and T. Gunnlaugsson, *Chem. Soc. Rev.*, 2010, **39**, 3936–3953.
25 H. Q. Dong, T. B. Wei, X. Q. Ma, Q. Y. Yang, Y. F. Zhang, Y. J. Sun, B. B. Shi, H. Yao, Y. M. Zhang and Q. Lin, *J. Mater. Chem. C*, 2020, **8**, 13501–13529.
26 J. W. Chen, C. M. Chen and C. C. Chang, *Org. Biomol. Chem.*, 2017, **15**, 7936–7943.
27 S. Banerjee, E. B. Veale, C. M. Phelan, S. A. Murphy, G. M. Tocci, L. J. Gillespie, D. O. Frimannsson, J. M. Kelly and T. Gunnlaugsson, *Chem. Soc. Rev.*, 2013, **42**, 1601–1618.
28 M. Poddar, V. Sharma, S. M. Mobin and R. Misra, *Chem. – Asian J.*, 2018, **13**, 2881–2890.
29 H.-H. Lin, Y.-C. Chan, J.-W. Chen and C.-C. Chang, *J. Mater. Chem.*, 2011, **21**, 3170.
30 H. Yu, Y. Guo, W. Zhu, K. Havener and X. Zheng, *Coord. Chem. Rev.*, 2021, **444**, 214019.
31 D. Gudeika, R. R. Reghu, J. V. Grazulevicius, G. Buika, J. Simokaitiene, A. Miasojedovas, S. Jursenas and V. Jankauskas, *Dyes Pigm.*, 2013, **99**, 895–902.

32 K. Liu, S. Tang, T. Wu, S. Wang, M. Zou, H. Cong and A. Lei, *Nat. Commun.*, 2019, **10**, 639.

33 I. Fdez. Galván, M. Elena Martín, A. Muñoz-Losa and M. A. Aguilar, *J. Chem. Theory Comput.*, 2009, **5**, 341–349.

34 D. Gudeika, A. Michaleviciute, J. V. Grazulevicius, R. Lygaitis, S. Grigalevicius, V. Jankauskas, A. Miasojedovas, S. Jursenas and G. Sini, *J. Phys. Chem. C*, 2012, **116**, 14811–14819.

35 D. Gudeika, R. R. Reghu, J. V. Grazulevicius, G. Buika, J. Simokaitiene, A. Miasojedovas, S. Jursenas and V. Jankauskas, *Dyes Pigm.*, 2013, **99**, 895–902.

36 H. El-Gezawy, W. Rettig and R. Lapouyade, *J. Phys. Chem. A*, 2006, **110**, 67–75.

37 T. Serevičius, R. Skaisgiris, J. Dodonova, I. Fiodorova, K. Genevičius, S. Tumkevičius, K. Kazlauskas and S. Juršėnas, *J. Phys. Chem. Lett.*, 2022, **13**, 1839–1844.

38 H. Beens, H. Knibbe and A. Weller, *J. Chem. Phys.*, 2004, **47**, 1183.

39 B. L. Cotts, D. G. McCarthy, R. Noriega, S. B. Penwell, M. Delor, D. D. Devore, S. Mukhopadhyay, T. S. De Vries and N. S. Ginsberg, *ACS Energy Lett.*, 2017, **2**, 1526–1533.

40 P. A. Panchenko, A. N. Arkhipova, O. A. Fedorova, Y. V. Fedorov, M. A. Zakharko, D. E. Arkhipov and G. Jonusauskas, *Phys. Chem. Chem. Phys.*, 2017, **19**, 1244–1256.

41 X. Sun, B. M. Chapin, P. Metola, B. Collins, B. Wang, T. D. James and E. V. Anslyn, *Nat. Chem.*, 2019, **11**, 768–778.

42 A. Samanta and G. Saroja, *J. Photochem. Photobiol., A*, 1994, **84**, 19–26.

43 M. L. Horng, J. A. Gardecki and M. Maroncelli, *J. Phys. Chem. A*, 1997, **101**, 1030–1047.

44 Y. Braver, A. Gelzinis, J. Chmeliov and L. Valkunas, *Chem. Phys.*, 2019, **525**, 110403.

45 I. H. M. Van Stokkum, D. S. Larsen and R. Van Grondelle, *Biochim. Biophys. Acta, Bioenerg.*, 2004, **1657**, 82–104.

46 M. Park, C. H. Kim and T. Joo, *J. Phys. Chem. A*, 2013, **117**, 370–377.